SLAC-PUB-9484
September 2002

Report of the Snowmass T4 Working Group on Particle Sources: Positron Sources, Antiproton Sources, and Secondary Beams

N. Mokhov* and S. Werkema
Fermilab, P.O. Box 500, Batavia, IL 60510

J. Sheppard
SLAC, Stanford, CA

V. Balbekov, Y. Batygin, L. Bellantoni, D. Casper, P. Cooper, S. Ecklund, Y. Efremenko, K. Flöttmann,
D. Harris, M. Hebert, P. Hurh, T. Inagaki, M. James, S. Kahn, H. Kirk, G. Lim, S. Maloy, A. Mikhailichenko,
G. Mills, B. Molzon, J. Morgan, T. Murphy, T. Nakaya, J. Norem, T. Omori, R. Partridge, R. Raja,
R. Samulyak, D. Schultz, N. Simos, M. Snow, W. Stein, A. Sunwoo, Z. Tang, H. White, A. Wolski, A. Zholents
(Dated: October 17, 2001)

This report documents the activities of the Snowmass 2001 T4 Particle Sources Working Group. T4 was charged with examining the most challenging aspects of positron sources for linear colliders and antiproton sources for proton-antiproton colliders, and the secondary beams of interest to the physics community that will be available from the next generation of high-energy particle accelerators. The leading issues, limiting technologies, and most important R&D efforts of positron production, antiproton production, and secondary beams are discussed in this paper. A listing of T4 Presentations is included.

Contents

---

*Electronic address: mokhov@fnal.gov

T4001

I.   INTRODUCTION

The T4 working group studied a wide variety of particle sources. While the technological issues confronted in the design and optimization of these disparate particle beams has some common features, the differences are significant. Consequently, this report is organized such that each particle source is treated separately. The major headings are those of the charge given to the group. The first part has to do with positron and antiproton sources, the second deals with secondary particle beams:

1. High performance positron sources will be required for the next generation of linear colliders. Antiproton sources are a source of antimatter for proton-antiproton colliders and can provide copious numbers of low energy antiprotons for fundamental research. Review the forefront technological issues in the development of the next generation of positron and antiproton sources. Examine in detail the most important and challenging aspects of these technologies, both from the point of view of performance and cost-effectiveness. What are the new ideas and avenues for sources? Prioritize the R&D efforts, in terms of the potential to provide maximal performance and/or cost-effectiveness; establish a technology-limited time line, and the resource requirements for the R&D efforts.

2. Although collider experiments dominate the current high-energy physics landscape, high intensity secondary beams of particles still form the basic tools for some important experiments. Review the leading issues and limiting technologies for the development of high-performance secondary beams potentially available from the next generation of high-energy particle accelerators. Identify the secondary beams of interest to the community. Identify the most important R&D efforts that could lead to significant advances in the performance of such secondary beams.

II.   POSITRON PRODUCTION FOR LINEAR COLLIDERS

A.   Performance and Main Issues

The next generation of linear colliders requires positron beams that are 20-60 times more intense than the SLC positron beam. In all of the designs, peak shock stress in the targets, average power dissipation, radiation damage, and collection efficiencies are major design considerations and are active areas of study. Polarized positron sources are seen as possible upgrade paths for the linear collider designs and are not included in any of the baseline configurations. Investigations into polarized positron production concentrate on the conversion of circularly polarized, high-energy photons. TableI lists various system parameters in the different designs; the SLC positron source parameters[1] are included for comparison. Annotated schematics of the CLIC[2], NLC[3], JLC[4], and TESLA[5] linear collider positron source designs are presented below.

TABLE I: Positron system parameters for the SLC, NLC, TESLA, JLC, and CLIC. Shown for targets are their length L, peak energy deposition q, average power absorption P and normalized acceptance ϵ.

System	Flux (e^+)	Target Material	L (r.l.)	q (J/g)	P (kW)	ϵ (m-rad)
SLC	$4.8{\times}10^{12}$	W_75Re_25	6	30	5	0.010
NLC	$1.8{\times}10^{14}$	W_75Re_25	4	40*	16*	0.045
TESLA	$2.8{\times}10^{14}$	Ti-alloy	0.4	222	5	0.048
JLC	$2.0{\times}10^{14}$	W-Re	6	140	49	0.027
CLIC	$1.0{\times}10^{14}$	W_75Re_25	4.5	65	22	0.027
JLC, pol	$1.0{\times}10^{14}$	W_75Re_25	0.6	13	0.5	0.060

(*) Energy deposition and absorbed power in each of 3 targets.

The NLC design for positrons is a conventional system in which positrons are produced by colliding 6.2 GeV electrons into thick (4 r.l.), high-Z material targets, capturing the resulting positrons, and accelerating them to the 1.98 GeV energy of the predamping ring system. Three targets are required to handle peak shock stress in the target; a predamping ring is necessary because of the large phase space area occupied by the collected positrons. The TESLA design utilizes a 100 m long planar undulator[6] to generate high-energy photons (in the range of 10 - 30 MeV). A thin (0.4 r.l.), titanium target is used for photon-positron conversion. The resultant positrons are collected, accelerated, and injected into the TESLA positron damping ring at 5 GeV; a predamping ring is not required in the TESLA design. JLC has a design for conventionally produced positrons that is very

similar to the NLC design but is based on a single target. The CLIC design is similar to both the NLC and JLC systems. JLC[7], NLC[8, 9], and TESLA[5] are considering polarized positron sources based on the conversion of circularly polarized, high energy photons.

Peak shock stress in the targets occurs on a time scale of microseconds. This is mitigated by increasing the incident beam size on the target (on the scale of 1 - 2 mm, rms). Increasing the incident beam size increases the emittance of the resultant positrons, reducing yield into a fixed collection acceptance. In the case of photon based production schemes high strength, low-Z, converter material can be used. On the other hand, high-Z targets are preferred for the conventional schemes. For any scheme, the need to maximize the phase space density of the generated positrons pushes the stresses in the targets to the failure limit. Development of high strength materials and the determination of stress limits (both theoretically and empirically) is of great importance. Temperature spikes dissipate on the time scale of milliseconds. Average power deposition in the targets is accommodated through target rotation and water cooling. While of considerable concern, the issue of average power dissipation is handled in this straightforward manner. Because of the high bunch rates, target degradation and failure due to radiation damage and thermal cycle fatigue must be considered in the overall system design. The topics of target shock stress, power dissipation, radiation and fatigue damage are active areas of research[10–14].

High field, solenoidal magnet systems are located immediately downstream of the target systems. The fields are in the range of 5-7 Tesla and are generated using a ∼1 Tesla DC solenoid in combination with a ∼5 Tesla pulsed flux concentrator. Development of stronger initial collection fields (∼10 Tesla) is of interest for improving the collection yields. The longer pulse lengths and larger apertures necessary for the next generation of flux concentrators require engineering development. It should be noted that the Muon Collider source calls for a 20 Tesla field around the target[15]. This is accomplished by using a pulsed Cu solenoid (7 Tesla) along with a 13 Tesla SC solenoid. This approach may be beneficial to the positron source designs.

NLC, TESLA, and CLIC use normal conducting L-band linac systems for the initial capture and acceleration of the positrons. After initial capture and acceleration to 200 MeV in room temperature copper structures, TESLA switches over to superconducting cavities for further acceleration to the damping ring energy. CLIC and NLC retain normal conducting L-band structures for the full acceleration. L-band provides larger transverse and longitudinal apertures and hence improved acceptance over an S-band design. The JLC design uses S-band RF for positron collection and acceleration.

Trade-offs between the energy and bunch charge of the electron drive beams are somewhat arbitrary. The product of drive beam energy and current are dictated by the expected yield calculations. CLIC uses a 2 GeV drive beam energy, JLC 10 GeV, and NLC 6 GeV. Target thickness is chosen according to the incident beam energy[16]. TESLA has taken a different approach by using the production electron beam to generate high-energy photons in an undulator located at the end of the TESLA electron main linac. The energy of this beam is variable between 150 GeV to 250 GeV according to the requirements of the scheduled physics program. The TESLA design must accommodate the variable photon spectrum.

None of the present linear colliders include polarized positron systems in their baseline designs. However, the JLC and TESLA design groups are developing such designs as possible upgrades. The basic idea is to produce circularly polarized photons at an energy of about 60 MeV. Pair creation in thin radiators preserves the helicity of the initial photons. Proper selection and transport of the resultant positrons can produce positron beams with a longitudinal polarization of about 60%. This scheme was first developed in the 1970-1980's at BINP[17] but has not been demonstrated. The TESLA scheme for polarized positrons utilizes a circular undulator to produce polarized photons. This approach follows a relatively straightforward path of replacing the planar undulator in their design with a short period helical undulator. TESLA positron polarization requires an undulator that is about 100 m in length and the installation of a photon collimator in front of the target. JLC has proposed a scheme in which circularly polarized photons are produced through Compton backscattering of circularly polarized laser beams off of 6 GeV electrons. The JLC scheme eases the requirements on the electron beam (6 GeV versus 150 - 250 GeV) used to produce photons, but presents a very large demand on the laser systems (∼400 kW of average laser power[18]). The collection schemes for either approach have the same functional requirements with regard to polarization selection from the positron flux even though the beam formats of the two designs are very different. The SLAC group is presently evaluating both schemes for application to the NLC.

B.   Schematics of the Positron Systems

1.   The NLC Positron Source

Positrons are produced by directing 6 GeV electrons into a 4 r.l. thick target of $W_{75}Re_{25}$ (Fig. 1). Three targets are required to handle the peak shock stress in the target material; the incident electron beam is divided amongst the targets with an RF deflector. Positrons are captured in a 7 Tesla peak field flux concentrator and accelerated to 250 MeV in a room temperature, L-band linac systems. The resultant three streams of positrons are combined at an energy of 250 MeV using another RF deflector. Further acceleration to 1.98 GeV is done with a room temperature L-band linac. The normalized acceptance of the capture channel (including predamping ring) is specified as 0.045 m-rad, edge.
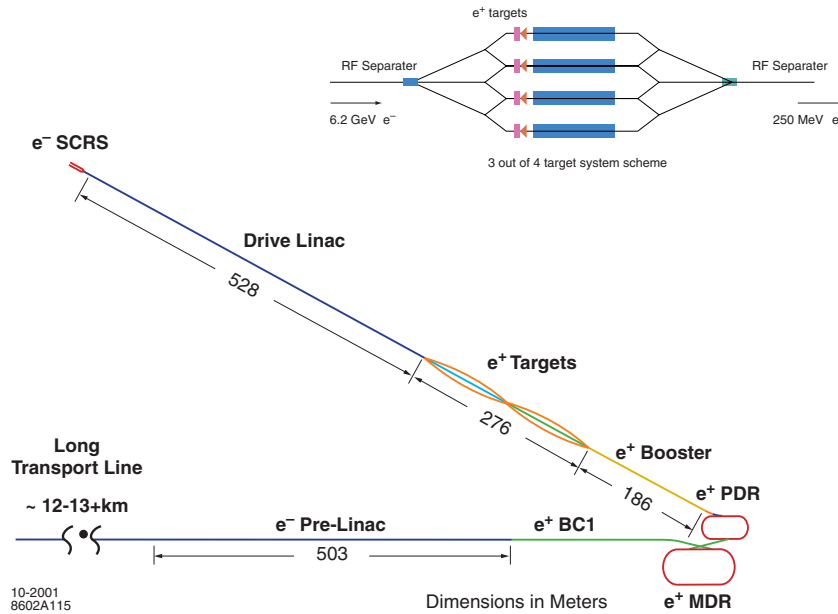
FIG. 1: NLC positron production scheme.

2.   The TESLA Positron Source

Positrons are produced from a 10-30 MeV photon beam in a 0.4 r.l. thick target of Ti-alloy. The photons are generated in a ~100 m long planar undulator which is located at the end of the TESLA electron main linac as shown in Fig. 2; the energy of the electron beam is variable in the range of 150-250 GeV. Positrons are captured in a 6 Tesla peak field flux concentrator and accelerated to 250 MeV in a room temperature, L-band linac system. Further acceleration to 5 GeV is done with a superconducting L-band linac. The normalized acceptance of the capture channel (including damping ring) is specified as 0.048 m-rad, edge.
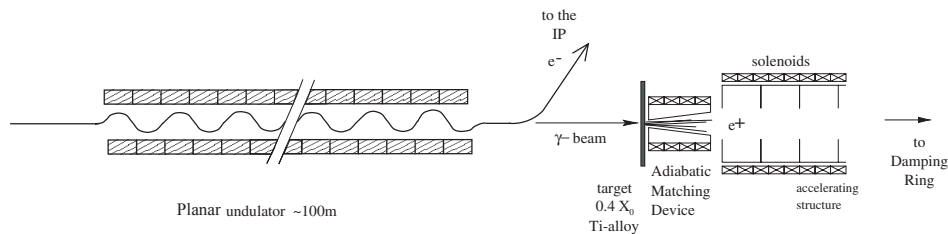
FIG. 2: TESLA positron production scheme.

3.   The JLC Positron Source System

Positrons are produced by directing 10 GeV electrons into 6 r.l. thick target of $W_{75}Re_{25}$. Positrons are captured in a 8 Tesla peak field flux concentrator and accelerated to 90 MeV in a room temperature, S-band linac system (Fig. 3). Acceleration to the predamping ring energy of 1.98 GeV is done with a S-band linac system. The normalized acceptance of the capture channel (including predamping ring) is specified as 0.027 m-rad, edge.
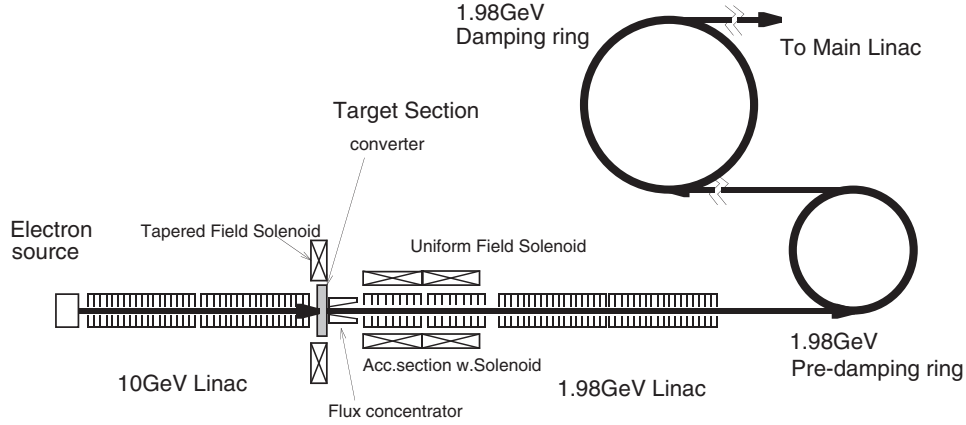

FIG. 3: Schematic of the JLC positron source.

4.   The CLIC Positron Source

Positrons are produced by directing 2 GeV electrons into 4.5 r.l. thick target of $W_{75}Re_{25}$. Positrons are captured in a 7 Tesla peak field flux concentrator and accelerated to 200 MeV in a room temperature, L-band linac system as shown in Fig. 4. Acceleration to the predamping ring energy of 1.98 GeV is done with a room temperature L-band linac system. The normalized acceptance of the capture channel (including predamping ring) is specified as 0.027 m-rad, edge.
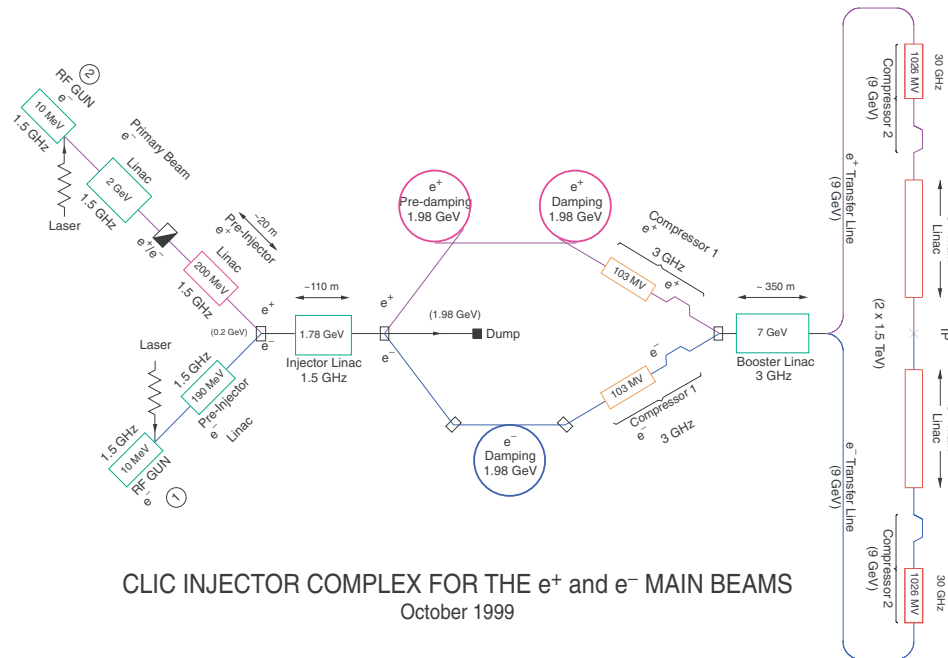

FIG. 4: Schematic of the CLIC positron source.

Positrons are produced from a 60 MeV circularly polarized photon beam in a 0.5 r.l. thick target of $W_{75}Re_{25}$ (Fig. 5). The photons are generated through Compton backscattering of circularly polarized laser beams off 6 GeV electrons. The peak power of the laser pulses is 73 GW and the average power of each of 50 lasers is 8 kW. 400 kW of total, average laser power is required. The normalized acceptance of the capture channel (including damping ring) is specified as 0.06 m-rad.
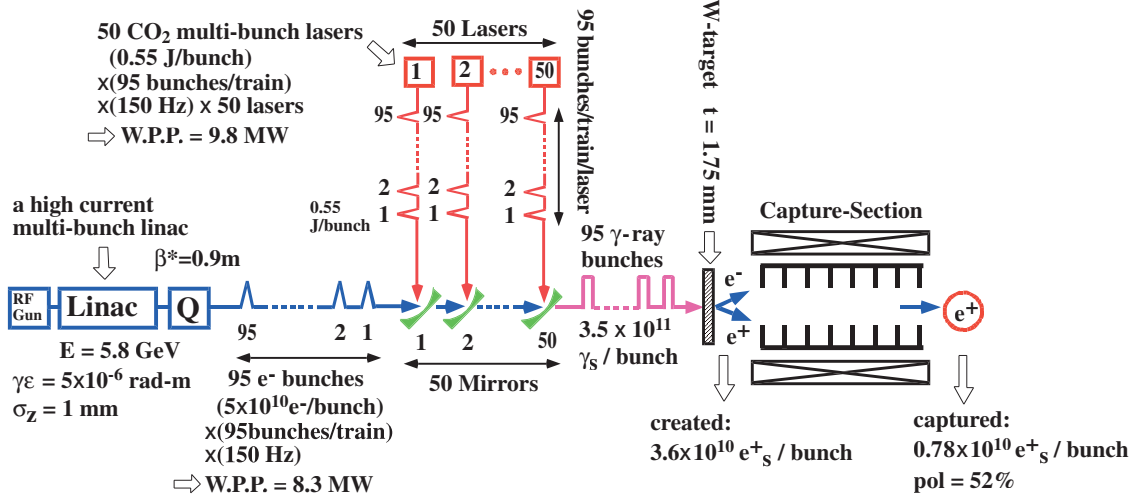

FIG. 5: Schematic design of the JLC polarized positron source.

III. ANTIPROTON PRODUCTION FOR PROTON-ANTIPROTON COLLIDERS

A. Antiproton Sources

At the present time there are two sources of antiprotons for the world's physics experiments: the CERN Antiproton Decelerator (AD) and the Fermilab Antiproton Source. These two facilities perform rather different functions. The Antiproton Decelerator functions as a relatively low intensity ($\sim 10^7$ $\bar{p}$/minute) source of low energy (5 MeV) antiprotons for experiments with anti-Hydrogen and antiprotonic Helium (ATHENA, ATRAP, and ASACUSA)[19]. The Fermilab Antiproton Source serves primarily as a source of high intensity ($\sim 10^{12}$ $\bar{p}$/store), bright (20πmm-mrad$\times 0.03\%$ $\Delta p/p$) antiprotons for the Tevatron Collider[20]. The T4 working group restricted its focus to the technological issues associated with the rate at which antiprotons can be accumulated at the Fermilab Antiproton Source.

The layout of the Fermilab Antiproton Source is shown in Fig. 6. Presently, the Fermilab Antiproton Source collects antiprotons at a rate of approximately 7.5×10^{10} $\bar{p}$/hour. Various improvements in the Fermilab accelerator complex over the next 3 to 5 years may increase the $\bar{p}$ accumulation rate to 52×10^{10} $\bar{p}$/hour[21]. Beyond that, the implementation of the Proton Driver[22] may further increase the $\bar{p}$ accumulation rate if the Antiproton Source can be made to accommodate the increased $\bar{p}$ flux.

The issues associated with increasing antiproton production fall into three basic categories:

1. Increasing the brightness of the protons on the $\bar{p}$ production target.

2. Increasing the acceptance of the antiproton collection and accumulation systems downstream of the target.

3. Increasing the $\bar{p}$ flux that can be transmitted by the momentum stacking system.

These three basic issues are briefly addressed below.

B. Increasing the Brightness of Protons on the $\bar{p}$ Production Target

The various means by which intense low emittance proton beams can be produced is a topic that lies outside the scope of the T4 charge. Increasing the brightness of the proton requires a concomitant target station
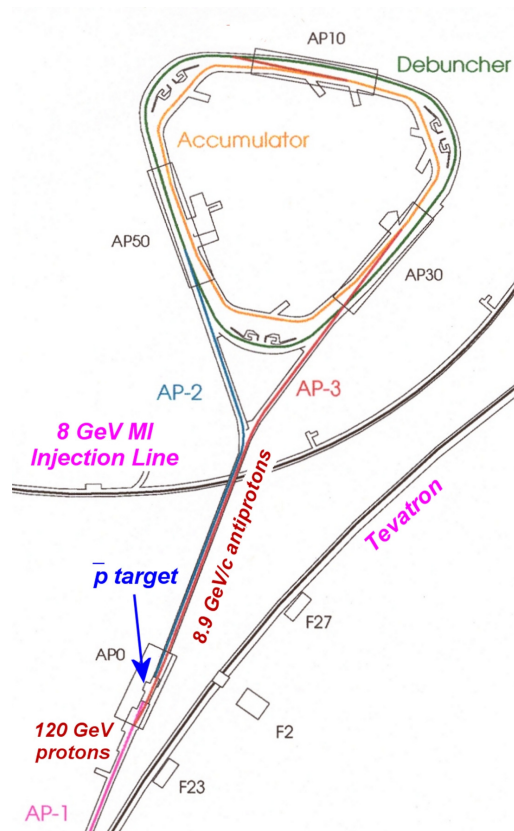
FIG. 6: Layout of the Fermilab Antiproton Source.

engineering effort to ensure that the target can withstand the consequent increase in energy deposited during each pulse. Table II gives the parameters of the incident proton beam at the Fermilab $\bar{p}$ production target. The increase in proton intensity and the decrease in spot size that are anticipated in the future will cause a significant increase in the energy deposited per pulse in the target.

TABLE II: Proton beam parameters at the Fermilab $\bar{p}$ production target.

Parameter	Present	After Run IIb upgrades
Intensity (ppp)	4.5×10^{12}	5.0×10^{12}
Cycle time (sec/pulse)	3.0	1.5
Pulse (μsec)	1.6	1.6
$\Delta p/p$ ($\pm\%$)	0.15	0.15
σ_x (mm)	0.14	0.1
σ_y (mm)	0.23	0.1

At present, the peak energy deposition in the nickel target of the Fermilab Antiproton Source is approximately 1000 Joules/gram for each incident pulse of proton beam (see Fig. 7). As is shown in Fig. 8, the resultant heating of the target material raises the temperature well beyond the melting point of copper and very close to the melting point of nickel ($\sim$2400°K). With the present configuration of the target station, there is very little margin available for further increases in proton brightness before steps must be taken to lower the energy deposited in the target.

When higher proton intensities are available, a beam sweeping system will be used distribute the incident pulse over an area on the target face that is 2-3 times the rms transverse size of the proton beam. A beam sweeping system has been built at Fermilab but has yet to be tested with beam. The beam sweeping system consists of a pair of magnets upstream of the target capable of producing a 625 kHz rotating dipole field that moves the beam in a 0.3 mm spiral on the face of the target. A sweeping magnet will also be installed downstream of the target to correct the trajectory error of the antiproton beam that results from sweeping the primary beam (see Fig. 9).
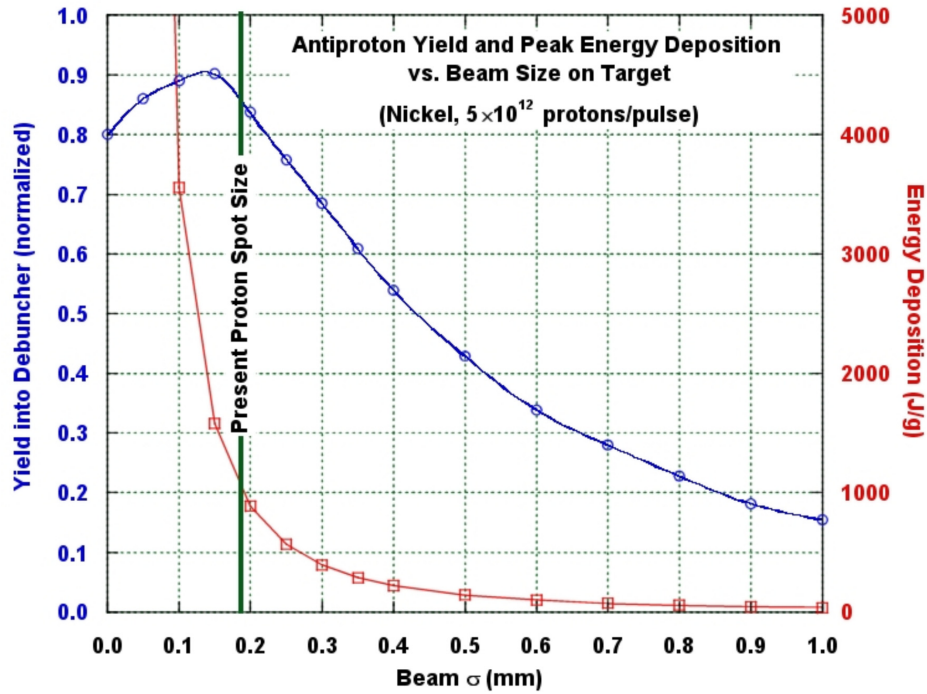
FIG. 7: Energy deposition and $\bar{p}$ yield versus spot size for a pulse of 5.0×10^{12} protons on a nickel target[23].
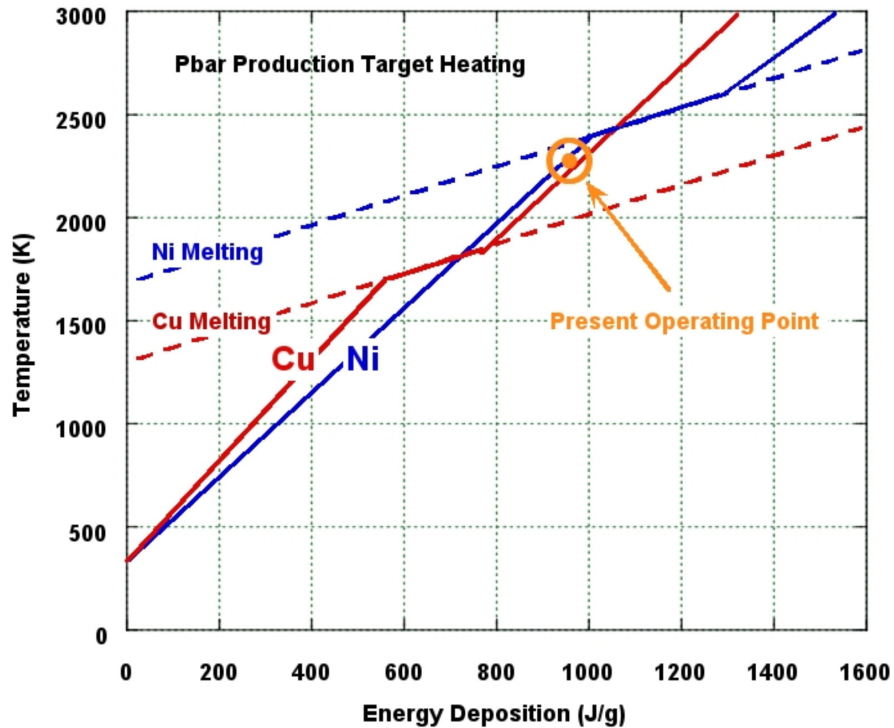

FIG. 8: Target heating as a function of energy deposited per incident proton pulse[23].

It is not yet known what reduction in target heating the beam sweeping system will achieve. Further reduction of the energy deposition must be accomplished by increasing the proton spot size. This, in turn, results in a reduction in antiproton yield. It is likely that significant target R&D will be required to design a $\bar{p}$ production target that can withstand the primary beams that will be available if the Proton Driver is built.
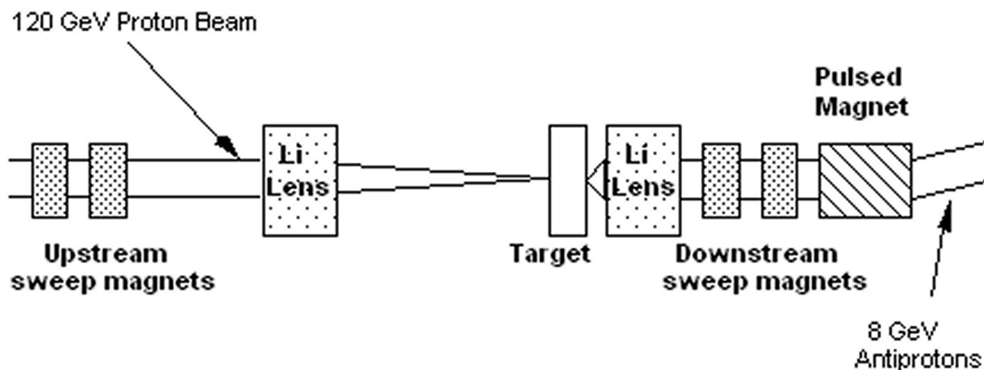
FIG. 9: Schematic representation of the Fermilab Antiproton Source target station showing the location of the upstream and downstream sweeping magnets.

C.   Increasing the Acceptance Downstream of the Target

The antiprotons produced in the target are focused with a collection lens. The Fermilab Antiproton Source target station utilizes a lithium collection lens (shown in Fig. 10). The lithium lens consists of a cylindrical lithium center conductor encased in a water-cooled titanium alloy septum. The lens was designed to be pulsed with a current of 670 kAmps, which gives a gradient of about 1000 Tesla/m.
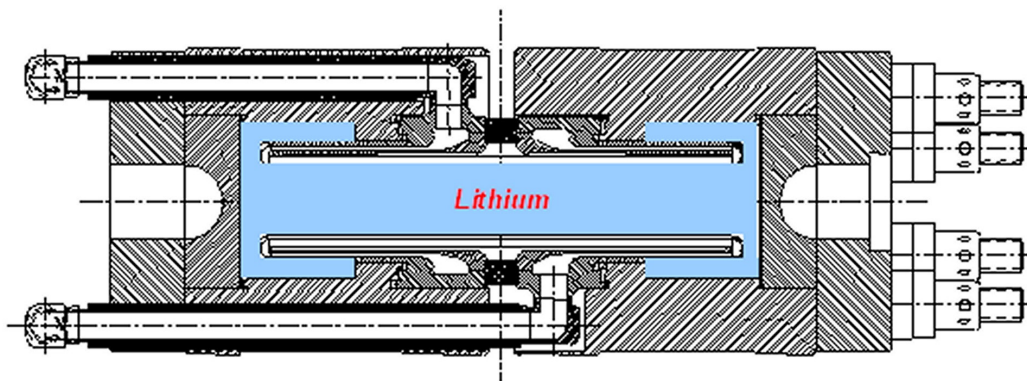

FIG. 10: Fermilab Antiproton Source Lithium Lens. The length is 14.5 cm. The radius of the beam aperture is 1 cm.

Increasing the gradient of the collection lens increases the antiproton yield (Fig. 11). Unfortunately, running at the design gradient is incompatible with long-term reliable operation of the lens. Experience has shown that a reduction in gradient to below 750 Tesla/m is required for a usefully long lithium lens lifetime ($\sim 5 \times 10^6$ pulses)[24]. This reduction in gradient reduces the antiproton yield by at least 20%. Since there is a significant gain in $\bar{p}$ yield to be had by raising the lens gradient, a significant amount of engineering effort has been devoted to understanding the failure modes of the lithium lens and to improving upon the mechanical design. A finite element analysis of the current lens design was recently completed[25, 26]. The results of this analysis indicate the possibility of a separation of the lithium from the septum wall during the magnetic pinch that occurs near the peak of its current pulse.

There are two projects underway aimed at improving upon the mechanical design of the lithium lens. The Budker Institute of Nuclear Physics in Novosibirsk is exploring the feasibility of manufacturing and operating a collection lens containing a lithium conductor in the liquid state. The liquid lithium is continuously recirculated through the body of the lens in an effort to distribute the stresses uniformly on the septum wall. To date, this effort has not produced a reliable lens capable of running at high gradients.

Fermilab has begun the design and construction of a new solid lithium lens prototype. The new design greatly reduces the number of joints in the septum structure. The manufacturing process will employ diffusion bonding technology for welding septum joints. These features result in a more uniform grain structure.
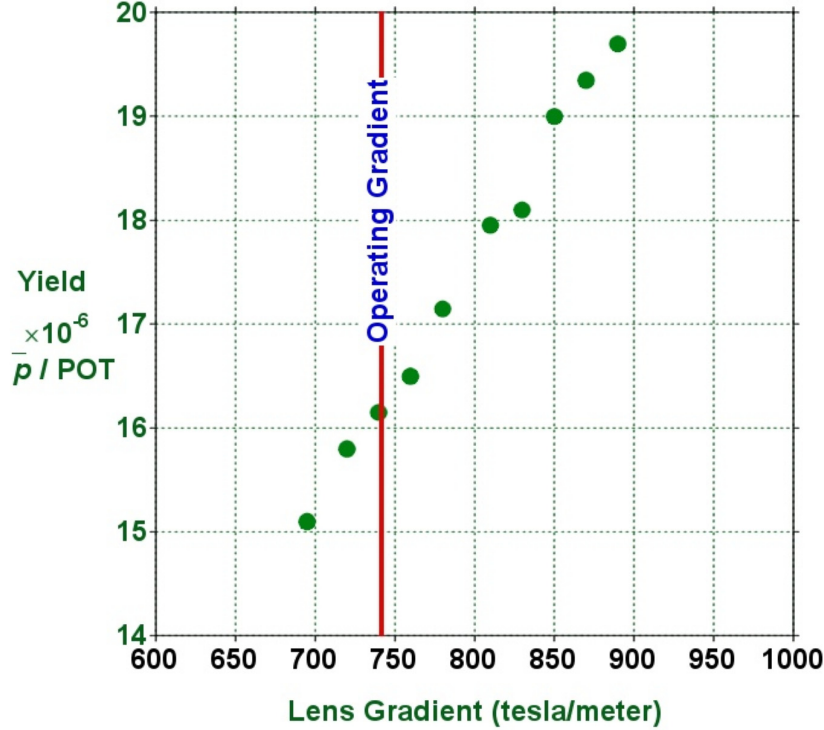
FIG. 11: Measured antiproton yield as a function of lithium lens gradient.

D.   Increasing the $\bar{p}$ Flux That Can be Transmitted by the Momentum Stacking System

The bottleneck for the transmission of increased $\bar{p}$ flux is the stochastic cooling system that accomplishes the momentum stacking of the antiprotons in the Antiproton Source Accumulator Ring. Fig. 12 shows the longitudinal distribution of the antiproton beam in the Accumulator. Beam is injected on the high-energy side of the momentum aperture, decelerated to the central orbit with RF, and then stochastically stacked into the core of the accumulated beam with the stacktail momentum cooling system. The stacktail cooling system must move each new pulse of antiprotons off of the central orbit prior to the arrival of the next pulse. Any beam that remains on the central orbit is phase displaced backwards by the RF bucket containing the next pulse of antiprotons.

The equilibrium energy distribution of the beam in the stacktail region of the profile is an exponential given by:

$$\Psi(E) = \Psi_0 \exp\left(\frac{E - E_0}{E_d}\right) \tag{1}$$

Fig. 13 illustrates the exponential character of the $\bar{p}$ longitudinal distribution. The slope of the distribution, E_d, determines the maximum flux (ϕ_{max}) that can be passed by the stacktail momentum cooling system. ϕ_{max} is given by:

$$\phi_{max} = \frac{|\eta| W^2 E_d}{4 f_0 pc \ln\left(f_{max}/f_{min}\right)} \tag{2}$$

where W is the bandwidth of the stacktail momentum cooling system, f_{min} and f_{max} are the band edges. Any increase in the $\bar{p}$ flux must, therefore, be accompanied by a commensurate increase in the gain slope (E_d) of momentum stacking system.

Increasing the gain slope, however, increases detrimental interactions between the momentum stacking system and the core of the accumulated $\bar{p}$ beam severely limiting the peak $\bar{p}$ intensity that can be accumulated. Consequently, any further increases in the $\bar{p}$ production rate will require another storage ring to which the Accumulator beam is transferred when its peak $\bar{p}$ intensity has been accumulated. The Fermilab Recycler Ring is presently being commissioned for this purpose. It is expected that the achievement of the antiproton production rates required for Collider Run II will necessitate the transfer of 20×10^{10} antiprotons approximately every 20
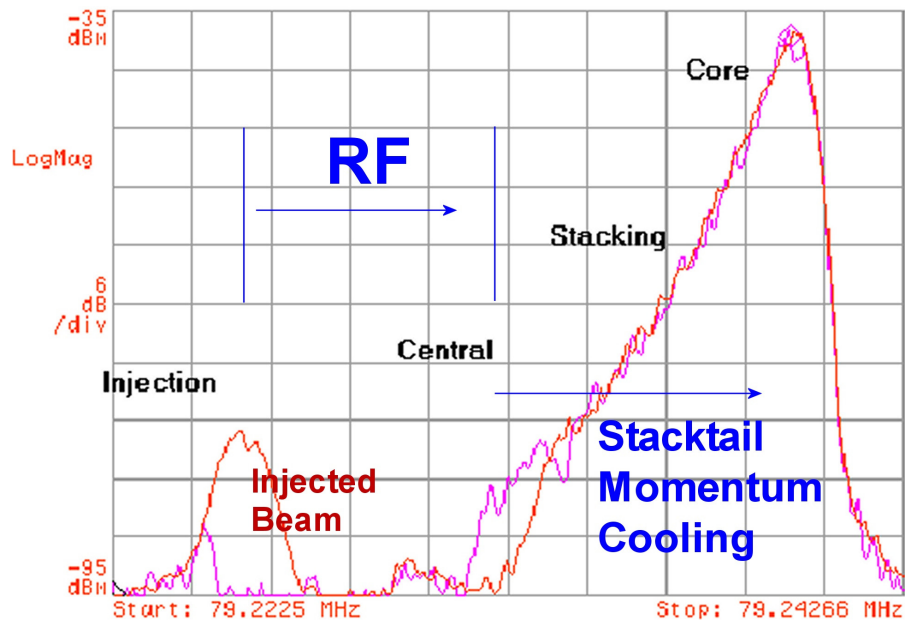
FIG. 12: Longitudinal profile of the $\bar{p}$ beam in the Antiproton Source Accumulator. The red trace shows a newly injected pulse of antiprotons on the injection orbit.
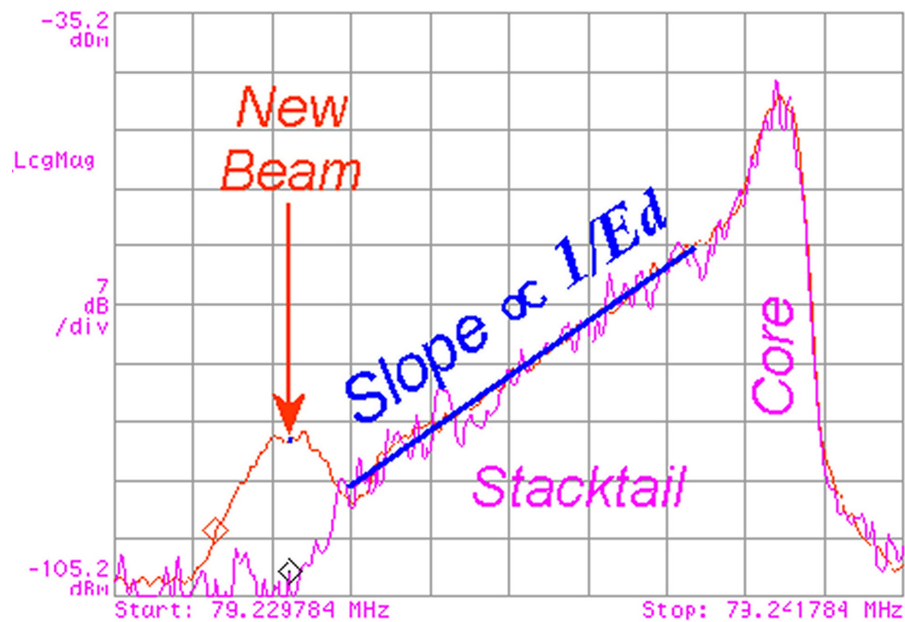

FIG. 13: Longitudinal $\bar{p}$ profile showing only the portion of the Accumulator momentum aperture between the central orbit and the core. The red trace shows a newly deposited pulse on antiprotons on the central orbit. The magenta trace shows the profile after the new pulse has been moved off of the central orbit by the stacktail momentum cooling.

minutes. Furthermore, increasing E_d causes the stacktail to occupy a larger portion of the momentum aperture of the accumulator. Thus, the momentum aperture of the Accumulator imposes an additional constraint on the maximum $\bar{p}$ flux attainable. Significant R&D will be required to extend this scenario to accommodate $\bar{p}$ fluxes greater than the $52 \times 10^{10} \bar{p}$/hour anticipated in Collider Run II.

IV. SECONDARY BEAMS FOR HIGH-ENERGY PHYSICS RESEARCH

The secondary beams of interest to the community include kaon, neutrino, muon and neutron beams. Muon beams are also of interest as a basis for neutrino factories and muon colliders. The range of proton beams used to generate secondary beams spans from a fraction of GeV to 1 TeV in energy and from 0.1 μA to 5 mA in beam current, as shown in Fig. 14. Common issues for high-intensity high-performance secondary beams include production and handling of high-power proton beams, targets that withstand such beams, secondary beam capture, focusing, separation and monitoring. Novel techniques have been proposed and are under development: liquid metal jet and rotated band targets, high field hybrid capture solenoids, superconducting RF beam separation, bent crystal channeling to extract and focus beams, etc. Substantial progress in simulation code development and comprehensive simulation studies as well as dedicated test experiments allow for a fast move.
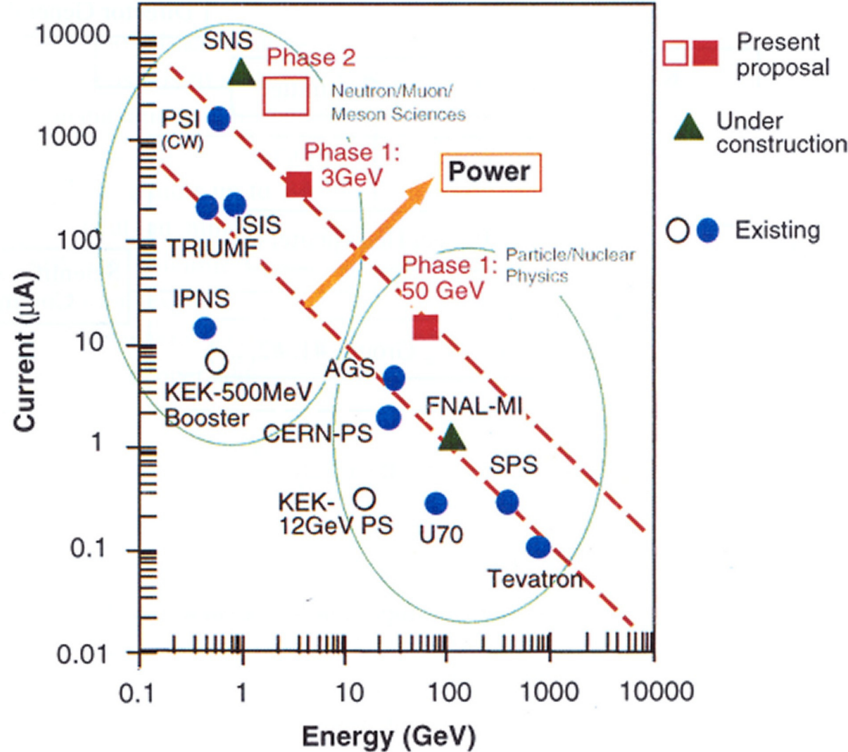

FIG. 14: Beam current and energy of existing, under construction, and proposed proton accelerators.

A. Kaon Beams

Kaon physics is alive, well and very active[27]. Existing and proposed experiments with secondary kaon beams include NA48/1/2 at CERN, KTeV and CKM at Fermilab, E787/E949 and KOPIO at BNL, E391a at KEK, and OKA at IHEP. As an example, Fig. 15 shows scheme of the CKM experiment with a K^+ beam[28]. The experiments aim at determination of CKM matrix elements and tests of chiral perturbation theory in rare kaon decays, search for T, CP and CPT symmetry violation, and other fundamental issues.

The field is quite mature with many precise, fancy, even elegant beam techniques in use and under development. The most impressive new beam technologies include: bent crystal channeling of machine protons to make a K_s^0 beam, "double band" beams with simultaneous K^+ and K^- beams, advanced collimation techniques to control beam tails, experiments driven by the entire output of the accelerator as if they were neutrino experiments ("proton blow-torches"), superconducting RF separated beams, and precision TOF for low energy neutral kaon beams. A principle of the kaon beam separation with superconducting RF is described in Fig. 16. These new techniques in kaon beam intensity, purity and time structure, although requiring further R&D work, are allowing a next generation of new experiments.
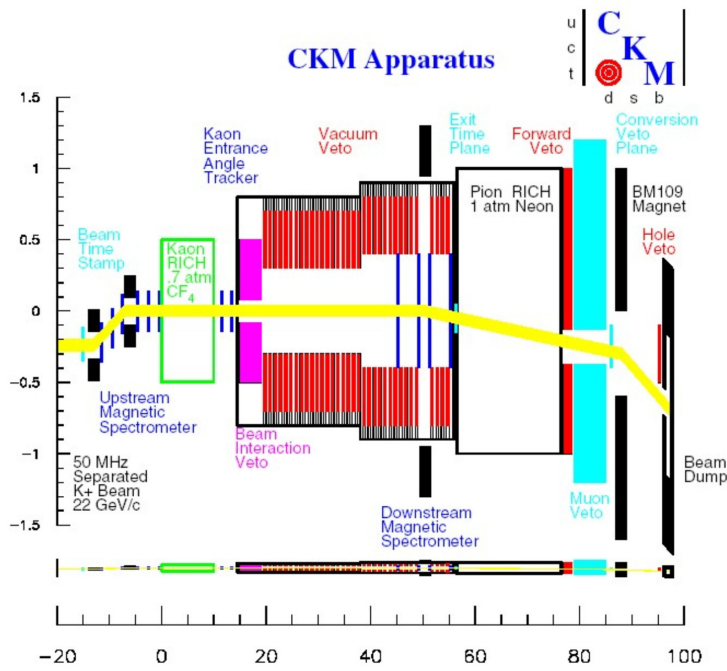
FIG. 15: Schematic view of the CKM experiment at Fermilab.

FIG. 16: Superconducting RF separation principle.

B. Neutrino Beams

The MiniBoone, MINOS, K2K, SuperK, SNO, Borexino, OPERA and ICANOE experiments will most likely confirm 3 generations of neutrino contributing to oscillations. To answer the remaining questions, a new generation of neutrino beams is needed. The leading issues here include[29]: appearance measurements, exploit

matter effects, neutrino and antineutrino beams separately, need two possible initial flavor beams - not just ν_μ with small ν_e contamination, superbeams, and neutrino beams generated in a muon storage ring.

Three types of conventional neutrino beams are considered: wide band beam, narrow band beam and quasi-monochromatic off-axis beam. Fig. 17 shows the principle and describes their advantages[30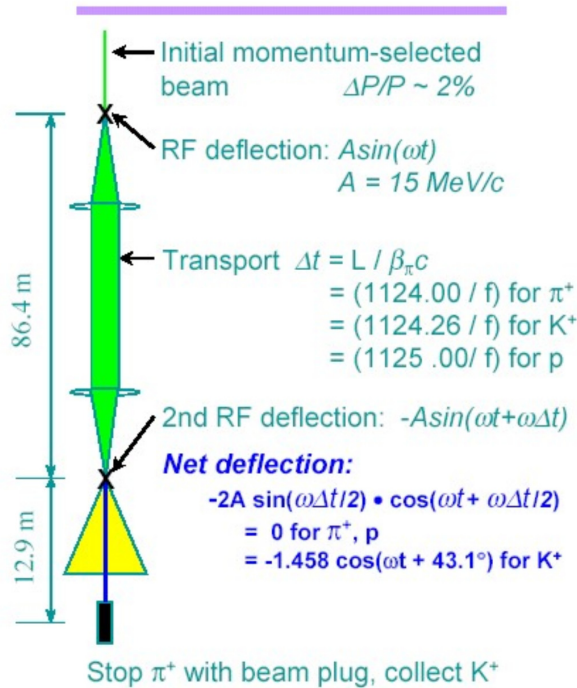]. Current proton beams are $<10^{13}$ ppp, future proton beams will be $>10^{14}$ ppp. The limiting aspects for neutrino production and beam lines are target integrity and lifetime, horn performance and lifetime, accurate alignment of the beam line to point to the far detector (GPS survey <0.01 mrad), beam control and long-term beam stability, beam monitoring (proton beam profile on target, muon beam profile at the muon pit and neutrino beam at the near detector). One can stay with "conventional" target technologies (a rod- or fin-like solid target) for proton beam power below 0.7-1 MW, and will need to switch to new ones (liquid metal jets, rotated band etc.) for higher beam powers.
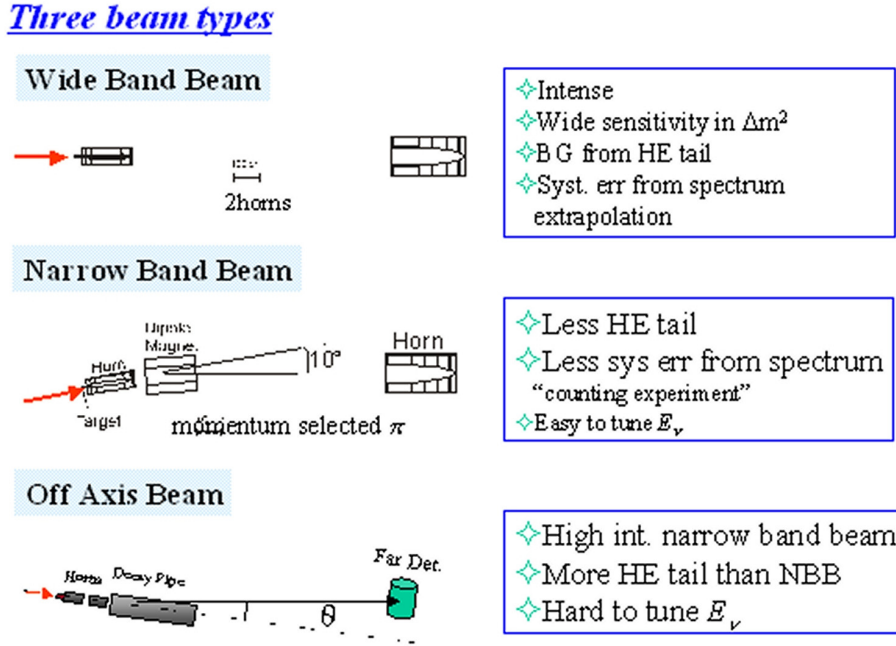

FIG. 17: Three types of neutrino beams.

Most challenging neutrino program is provided at a Neutrino Factory based on a muon storage ring with about 5×10^{20} muon decays per year in a straight section for a 4 MW proton beam. This approach is described in detail in the M1 Working Group summary. Unique possibilities are also provided at the 2 MW Spallation Neutron Source that will produce almost 10^{15} neutrinos in 60 Hz pulses (ORLanND proposal). That will make it the most intense, pulsed, intermediate energy neutrino source in the world[31]. The pulsed source would drastically reduce backgrounds from cosmic rays. It would also allow separation of ν_μ from $\overline{\nu}_\mu$ and ν_e, with well known spectra for each type. Intensity of $\overline{\nu}_e$ is severely suppressed: $\overline{\nu}_e/\overline{\nu}_\mu = 3 \times 10^{-4}$. This facility will be large enough to host one large 2 kt detector and several smaller 50-100 t detectors. Such a facility will give possibilities for: search for neutrinos oscillations, study of neutrinos intrinsic properties, precise measurement of elastic ν_e scattering, measurements of νN interactions in the energy scale relevant for solar physics and astrophysics.

To take the next step, we need more intense proton sources, targets that withstand high-intensity beams, horns and other focusing devices which survive in very close proximity to the target, totally new ideas about focusing to get narrow band beams with high fluxes.

C. Muon Beams

A very interesting experiment, MECO – a lepton flavor violation search experiment[32], is under construction at BNL (Fig. 18). Its goal is to detect coherent μN$\rightarrow e$N conversion with single event sensitivity $<2 \times 10^{-17}$. An intense pulsed muon beam will be derived from the AGS 7.9 GeV proton beam of 4×10^{13} p/s. A very elegant production and collection system based on superconducting solenoids will provide a 50 ± 20 MeV muon beam of 10^{11} μ/sec. Muons are brought to rest in thin target foils where they form muonic atoms in the 1s state.

Maximizing the integrated muon luminosity in the above energy range is the primary goal of the MECO muon beam. All possible sources of background are considered and measures taken to drastically suppress them. The MECO goal is to complete construction in early 2006 and begin production running late in that year with the world's most intense muon beam. The MECO ideas in targeting, capturing and particle transport can certainly be used in other applications with muon and other secondary beams.
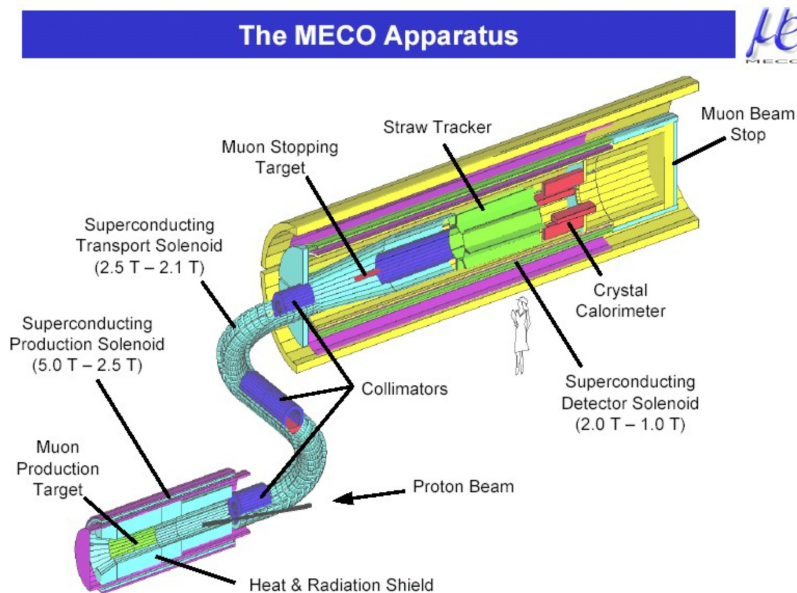

FIG. 18: The MECO experiment schematic view.

Stages 2 and 3 of the neutrino factory/muon collider plan (see the M1 Working Group summary), call for 0.2 and 2.5 GeV muon beams to be used directly and as a source of intense neutrino beams. They can provide up to 1.7×10^{21} decays per year with a 4 MW proton driver. The two most technologically challenging techniques to make high-quality muon beams - ionization cooling and optical stochastic cooling[33–35] – have been considered in detail at the T4 Working Group meetings.

D.   Neutron Beams

Low energy neutrons from reactors and spallation sources are used to conduct measurements of interest to particle physics and astrophysics. Examples include[36]: neutron beta decay studies (neutron decay rate for Big Bang nucleosynthesis, measurement of the V_{ud} element of the CKM matrix and tests of the matrix unitarity, searches for right-handed weak currents, searches for non -SM T violation), searches for T violation (neutron electric dipole moment, neutron optics) and B violation (neutron-antineutron oscillations), and neutron weak interactions with protons and light nuclei (low energy QCD tests). In the next decade this activity, if supported, is capable of measuring V_{ud} to 300 ppm, reducing the limit on the neutron EDM and neutron-antineutron oscillations by 3 orders of magnitude, and determining the neutron-proton weak interaction at low energy to 10%, among other things.

Progress in this field depends on access to intense neutron sources. Leading institutions planning to pursue this activity in the next 10-20 years include: ILL(France), FRM (Germany), PSI(Switzerland)), NIST (USA), LANSCE (USA), SNS (USA), JHF (Japan), ESS (not decided), and possibly FNAL (USA). Facilities come in two major types at both reactors and spallation sources: (1) neutron beams, (2) sources of ultra cold neutrons (UCN) which are essentially gas-like sources. For beam facilities, Table III gives a list of typical fluxes for a selection of existing and proposed sources.

The θ_c parameter describes the reflectivity of neutron guide tubes. Since reactor sources are CW whereas spallation sources are pulsed at 20-60 Hz, time-averaged flux is not the only criterion for the choice of the best source for a particular experiment. For UCN the main existing sources are ILL ($\sim$50 UCN/cc density in an external bottle) and LANSCE ($\sim$100 UCN/cc) with others in the planning stages at FRM and PSI. In addition there are "internal" UCN sources using superfluid ^{4}He (NIST, ILL) in which the experiments are done without extraction from the UCN moderator.

TABLE III: Typical neutron fluxes for various sources.

Facility	Neutron guide	Time-averaged flux (n/sec)
SNS, 2 MW, 60 Hz	$3\times\theta_c$, 10 cm$\times$12 cm	4×10^{11} (calculation)
LANSCE, 160 kW, 20 Hz	$3\times\theta_c$, 10 cm$\times$10 cm	6×10^{10} (calculation)
LLH113 (exists, new)	$3\times\theta_c$, 6 cm$\times$20 cm	1×10^{12} (measurement)
NIST NG6 (exists)	$1\times\theta_c$, 6 cm$\times$15 cm	1×10^{11} (after upgrade)

E.   Targetry

A list of targetry issues includes[15] particle production, collection and monitoring, background suppression and control, target and capture component integrity and lifetime, superconducting coil quench stability, heat loads, radiation damage and activation of materials near the beam, spent proton beam handling, and numerous shielding issues from prompt radiation to ground-water activation. A typical target station configuration as implemented in the MARS[37] model for a Neutrino Factory is shown in Fig. 19. All these issues are addressed in active R&D efforts: novel designs for high-performance secondary beams, shower simulation code developments and studies, thermal and stress analysis, magnetohydrodynamic analysis, instrumentation for target shocks, target experiments (E951 at BNL), particle production experiments (E910 at BNL, HARP at CERN and P-907 at FNAL).
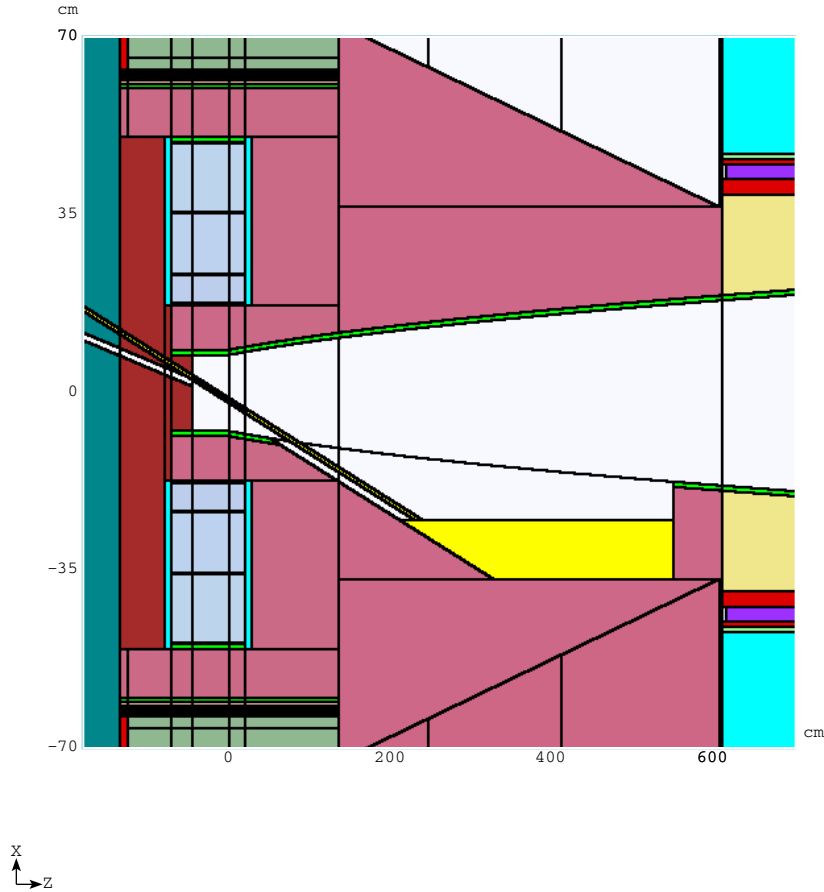
FIG. 19: A fragment of the MARS model of a Neutrino Factory target/capture system with tilted proton beam and mercury jet.

The current versions of shower simulation codes – MARS (FNAL) and FLUKA (CERN) – are quite adequate to tackle all of the above problems. The reliable performance of these codes have been demonstrated in numerous accelerator, detector and shielding applications at Fermilab, BNL, CERN, KEK, JAERI and other centers as well as in special benchmarking studies. One should be careful with use of two other general purpose codes

(GEANT and MCNPX) for the above targetry issues: quality of hadron-nucleus event generators in a wide energy range in both codes and absence of magnetic field treatment in MCNPX are still of a serious concern. A recent BNL E910 experimental data on inclusive pion and kaon production on nuclei are in excellent agreement with MARS predictions. The P-907 experiment[38] is proposed at Fermilab to measure the identities and momenta of particles produced in $\pi^{\pm}, K^{\pm}, p^{\pm}$ interactions on various nuclear targets and hydrogen as a function of beam momentum from 5 to 120 GeV/c with high statistics. It will also study hadronic fragmentation and, in particular, test the scaling law of particle fragmentation, search for exotic resonance such as glueballs, measure nuclear scaling, RHIC physics, and other service measurements.

A very powerful magnetohydrodynamics code, FronTier, has been developed at BNL and was discussed at the T4 working group[39]. Its numerical approach is based on the method of front tracking for numerical simulation of magnetohydrodynamic flows in discontinuous media. The FronTier MHD code was used first for numerical simulation of thin conducting liquid jets in strong non-uniform magnetic fields and demonstrated a big influence of the electromagnetic forces on the instability of jets in the region of non-uniform magnetic field behind the solenoid. To simulate behavior of a muon collider liquid mercury target in a high-field solenoid, using MARS-calculated energy deposition distribution in jet impinged by a 16 GeV proton beam, a tabulated equation of state for mercury was created in a wide temperature-pressure domain which includes the liquid-vapor phase transition and the critical point. The corresponding isentropic analytic EOS was also developed. Numerical simulation was performed for a 120μsec time interval. It turns out that the mercury target will be broken into a set of droplets due to the proton energy deposition and the radial velocity of the jet surface before the droplet formation is in the range 10-50 m/sec.

An interesting targetry experiment, E951, has been recently completed at BNL[40] to test mercury and graphite targets within the Muon Collider/Neutrino Factory project, with the AGS intensity up to 1.6×10^{13} ppp and the beam spot of as low as 0.5 mm RMS sigma. The goal was to find best possible materials that can be used as beam windows under such extreme conditions, to measure responses of the selected materials, to validate the prediction models against measurements, and to use the experimental results to benchmark energy deposition predicted by MARS, GEANT and MCNPX. Overall, E951 produced valuable results that, when fully analyzed, can shed light on a number of technical issues associated with solid targets, liquid targets and beam windows. The measured material response (thermal shock and attenuation in targets and beam windows and failure conditions) is reproduced quite satisfactory with the ANSYS code. Preliminary assessments show that MARS and GEANT estimations are in excellent agreement with the response of the ATJ graphite target.

A positron target made of W_74Re_26 surrounded by a silver-cooling jacket has been analyzed after irradiation with 30 GeV electrons at SLAC[41]. Initially, the target and its engine were shipped to hot cells at Los Alamos National Laboratory. The target was carefully removed from the engine using remote operations. Next, the target was leak tested and analyzed using optical microscopy. Then, the target was sliced into smaller pieces and polished for observation at higher magnifications and hardness testing. Analysis showed where a leak was formed during operation and significant cracking in the W_74Re_26 and the silver jacket on the exit side of the target. Hardness tests in the W_74Re_26 on the exit side revealed increases of over a factor of two greater than the original hardness. Such information is essential in the design of future accelerators that may run a higher power such as the Next Linear Collider.

F. Bent Crystals

The steering of beams with channeling by a bent crystal[42] has been demonstrated at Dubna, IHEP at Protvino, CERN, and Fermilab. A practical application of the technique has been splitting off a small fraction of an extracted beam to send to another target. This has been done at both CERN and IHEP. Dubna, IHEP, CERN, and Fermilab have extracted beams from the circulating beam. The highest extraction efficiency (defined as the ratio of the number of protons extracted to the total number of protons lost from the machine because of the crystal) measured to date is 85% at IHEP.

Future possible practical applications being planned are both extraction to experiments and as a replacement for the thin prescatterer in the standard halo collimation systems in circular accelerators. The bent crystal "scatters" the halo in one direction only and puts it deep into the long steel collimator that follows. The virtue of this technique has been demonstrated at IHEP. It is definitely planned for RHIC and is being considered for the Tevatron, LHC, and the Spallation Neutron Source. Extraction of halo beam to experiments is being considered at the AGS and COSY.

V.   LIST OF TALKS

1. S. Werkema (FNAL), "Antiproton Production Overview".

2. S. Ecklund (SLAC), "Positron Production Overview".

3. P. Cooper (FNAL), "Kaon Beams Overview".

4. D. Harris (FNAL), "Neutrino Beams Overview".

5. N. Simos (BNL), "BNL E951 Target Experiment Experience".

6. J. Norem (ANL), "Instrumentation for Target Shocks".

7. M. James (LNAL), "Radiation Damage".

8. S. Maloy (LANL), "Analysis of a Tungsten/Rhenium Target used at SLAC".

9. A. Sunwoo (LLNL), "Characterization of W-Re Material".

10. W. Stein (LLNL), "Thermal Stress Dynamic Structural Analyses of the SLC Positron Target".

11. N. Mokhov (FNAL), "Neutrino Factory Targets".

12. J. Morgan (FNAL), "Fermilab Antiproton Source Target Station Issues".

13. P. Hurh (FNAL), "The Path to a High Gradient Solid Lithium Collection Lens: Mechanical Engineering Issues".

14. N. Mokhov (FNAL), "Particle Interactions with Matter (MARS)".

15. Z. Tang (FNAL), "Thermal and Stress Analysis (ANSYS)".

16. R. Samulyak (BNL), "Muon Collider Target: Hydrodynamic and Magnetohydrodynamic Analysis".

17. S. Kahn (BNL), "Calculations of Energy Deposition in the E951 Carbon and Mercury Targets using MARS and GEANT".

18. D. Schultz (SLAC), "The NLC Positron Source".

19. K. Flöttmann (DESY), "The TESLA Positron Source".

20. Yu. Batygin (SLAC), "Polarized Positrons: Production and Collection".

21. T. Omori (KEK), "A Concept of a Polarized Positron Source for a Linear Collider".

22. A. Mikhailichenko (Cornell), "Polarized e^+e^- Production Based on Conversion of Gammas, Obtained from a Helical Undulator".

23. R. Partridge (Brown U.), "Compton Selection to Polarize e^+".

24. T. Nakaya (Kyoto U.), "Neutrino Beams in Japan".

25. G. Mills (LANL), "The MiniBoone Neutrino Beam".

26. Yu. Efremenko (U. Tenn./ORNL), "Neutrino Beams at the SNS".

27. D. Casper (UCI), "Oscillation Studies with Neutrino Super-Beams".

28. L. Bellantoni and H. White (FNAL), "K^+ Beams: CKM at Fermilab".

29. G.Y. Lim (KEK), "Kaon Beams in Japan".

30. M. Hebert (UCI), "The MECO Muon Beam".

31. V. Balbekov (FNAL), "Muon Cooling Channel, Ionization Cooling".

32. C.T. Murphy (FNAL), "Bent Crystal Beam Extraction and Focusing".

33. R. Raja (FNAL), "Secondary Beams in Experiment P-907".

34. A. Zholents (LBNL), "Optical Stochastic Cooling".

35. A. Wolski (LBNL), "Electron/Positron Damping: Radiation Damping in Practice".

[1] P. Krejcik, et al., "Recent Improvements in the SLC Positron System Performance", Proc. 3rd EPAC, Berlin, 1992 (also SLAC-PUB-5786, March 1992).

[2] T. Kamitani and L. Rinolfi, "Positron Production at CLIC", CLIC Note 465, December 2000.

[3] *2001 Report on the Next Linear Collider*, SLAC-R-571, June 2001.

[4] *JLC Design Study*, KEK Report 97-1, April 1997.

[5] *Conceptual Design of a 500 GeV e^+e^- Linear Collider with Integrated X-ray Laser Facility (TESLA Design Report)*, DESY 1997-048, May 1997.

[6] K. Flöttmann, "The TESLA Positron Source", Snowmass 2001 T4 presentation, July 2001.

[7] T. Hirose et al., "Polarized Positron Source for a Linear Collider, JLC", Nucl. Instr. and Meth., **A455**, 2000.

[8] Y. Batygin, "Positron Production and Collection", Snowmass 2001 T4 presentation, July 2001.

[9] D. Schultz, "The NLC Positron Source", Snowmass 2001 T4 presentation, July 2001.

[10] W. Stein, et al., "Thermal Shock Analysis Structural Analysis of a Positron Target", submitted to the proceedings of Particle Accelerator Conference 2001, Chicago, Illinois, 18-22 June, 2001.

[11] V. Bharadwaj, et al., "Analysis of Beam-Induced Damage to the SLC Positron Production Target", submitted to the proceedings of Particle Accelerator Conference 2001, Chicago, Illinois, 18-22 June, 2001.

[12] A. Sunwoo, "Characterization of W-Re Material", Snowmass 2001 T4 presentation, July 2001.

[13] M. Caturla, Private Communication, May 2001.

[14] M. James, "Radiation Damage", Snowmass 2001 T4 presentation, July 2001.

[15] N. Mokhov, "Particle Production and Radiation Environment at a Neutrino Factory Target Station", Fermilab-Conf-01/134, June 2001.

[16] S. Ecklund, "Positron Sources", Snowmass 2001 T4 presentation, July 2001.

[17] A. Mikhailichenko, "Polarized e^+e^- Production Based on Conversion of Gammas, Obtained from Helical Undulator", Snowmass 2001 T4 presentation, July 2001.

[18] T. Omori, "Compton Based Polarized Positron Source for the JLC", Snowmass 2001 T4 presentation, July 2001.

[19] P. Belochitskii, et. al., "Commissioning and First Operation of the Antiproton Decelerator (AD)", submitted to the proceedings of Particle Accelerator Conference 2001, Chicago, Illinois, 18-22 June, 2001. CERN/PS 2001-047 (AE).

[20] During the past 10 years there has also been a number of high energy physics experiments located in the Antiproton Source accumulator. These experiments consist of a series of Charmonium spectroscopy experiments (E760 and E835), a $\bar{p}$ lifetime experiment (APEX - E868), and an anti-hydrogen experiment (E862).

[21] *Plans for Tevatron Run IIB*. An unpublished preliminary design report. Table 2-1. Available on the Internet at: http://cosmo.fnal.gov/run2b/Documents/riibshort.pdf.

[22] W. Chou, et. al., *The Proton Driver Design Study*, FERMILAB-TM-2136, December 2000.

[23] J. Morgan, "FNAL Target Station Issues", Snowmass 2001 T4 presentation, July 2001.

[24] P. Hurh, "The Status and Future of Collection Lens Technology at the FNAL Antiproton Source", Snowmass 2001 T4 presentation, July 2001.

[25] P.G. Hurh, Z. Tang, "FEA Analysis of the AP-0 Target Hall Collection Lens (Current Design)", Fermilab Pbar Note 663, June 22, 2001.

[26] Z. Tang, "ANSYS Thermal and Stress Analysis", Snowmass 2001 T4 presentation, July 2001.

[27] P. Cooper, "Kaon Beams Overview", Snowmass 2001 T4 presentation, July 2001.

[28] L. Bellantoni and H. White, "K^+ Beams: CKM at Fermilab", Snowmass 2001 T4 presentation, July 2001.

[29] D. Harris, "Neutrino Beams Overview", Snowmass 2001 T4 presentation, July 2001.

[30] T. Nakaya, "Neutrino Beams in Japan", Snowmass 2001 T4 presentation, July 2001.

[31] Y. Efremenko, "Neutrino Beams at the SNS", Snowmass 2001 T4 presentation, July 2001.

[32] M. Hebert, "The MECO Muon Beam", Snowmass 2001 T4 presentation, July 2001.

[33] V. Balbekov, "Muon Cooling Channel, Ionization Cooling", Snowmass 2001 T4 presentation, July 2001.

[34] A. Zholents, et. al., "Halo Particle Confinement in the VLHC Using Optical Stochastic Cooling", Proceedings of EPAC 2000, pp. 262-264, Vienna, Austria, June 2000.

[35] A. Zholents, M. Zolotorev, and W. Wan, "Optical Stochastic Cooling of Muons", Phys. Rev. ST Accl. Beams, **4**, 031001, 2001.

[36] M. Snow, "Neutron Beams", contribution to Snowmass 2001 T4 group, July 2001.

[37] N.V. Mokhov, "The MARS Code System User's Guide", Fermilab-FN-628 (1995); N.V. Mokhov, O.E. Krivosheev, "MARS Code Status", Fermilab-Conf-00/181 (2000); http://www-ap.fnal.gov/MARS/

[38] R. Raja, et. al., "P-907: Proposal to Measure Particle Production in the Meson Area Using Main Injector Primary and Secondary Beams", May 2000; http://ppd.fnal.gov/experiments/e907/Proposal/p907.ps.

[39] R. Samulyak, "Muon Collider Target: Hydrodynamic and Magnetohydrodynamic Analysis", Snowmass 2001 T4 presentation, July 2001.

[40] N. Simos, "BNL E951 Target Experiment Experience", Snowmass 2001 T4 presentation, July 2001.

[41] S. Maloy, "Analysis of a Tungsten/Rhenium Target used at the Stanford Linear Collider Center", Snowmass 2001 T4 presentation, July 2001.

[42] C.T. Murphy, "Bent Crystal Beam Extraction and Focusing", Snowmass 2001 T4 presentation, July 2001.